

CONF-880676--1

DEVELOPMENT OF ENCAPSULATED LITHIUM HYDRIDE
SINK-SIDE THERMAL ENERGY STORAGE FOR
PULSED SPACE POWER SYSTEMS

D. G. Morris
J. P. Foote*
M. Olszewski
J. W. Whittaker†
Oak Ridge National Laboratory†
Oak Ridge, Tennessee 37831

For Presentation at the
AIAA Thermophysics, Plasmadynamics, and Lasers Conference
San Antonio, TX
June 27-29, 1988

CONF-880676--1

DE88 011496

DISCLAIMER

This report was prepared as an account of work sponsored by an agency of the United States Government. Neither the United States Government nor any agency thereof, nor any of their employees, makes any warranty, express or implied, or assumes any legal liability or responsibility for the accuracy, completeness, or usefulness of any information, apparatus, product, or process disclosed, or represents that its use would not infringe privately owned rights. Reference herein to any specific commercial product, process, or service by trade name, trademark, manufacturer, or otherwise does not necessarily constitute or imply its endorsement, recommendation, or favoring by the United States Government or any agency thereof. The views and opinions of authors expressed herein do not necessarily state or reflect those of the United States Government or any agency thereof.

*Postgraduate student, University of Tennessee Space Institute,
Tullahoma, TN 37388.


†Oak Ridge Y-12 Plant.

†Operated by Martin Marietta Energy Systems, Inc. under contract
No. DE-AC05-84OR21400 with the U.S. Department of Energy.

Work performed by Martin Marietta Energy Systems, Inc. under contract No. DE-AC05-84OR21400 with the U.S. Department of Energy for the Air Force Wright Aeronautical Laboratories under Interagency Agreement No. 1656-1508-A1.

The submitted manuscript has been authored by a contractor of the U.S. Government under Contract DE-AC05-84OR21400. Accordingly, the U.S. Government retains a nonexclusive, royalty-free license to publish or reproduce the published form of this contribution, or allow others to do so, for U.S. Government purposes.

MASTER

DISTRIBUTION OF THIS DOCUMENT IS UNLIMITED 

DISCLAIMER

This report was prepared as an account of work sponsored by an agency of the United States Government. Neither the United States Government nor any agency Thereof, nor any of their employees, makes any warranty, express or implied, or assumes any legal liability or responsibility for the accuracy, completeness, or usefulness of any information, apparatus, product, or process disclosed, or represents that its use would not infringe privately owned rights. Reference herein to any specific commercial product, process, or service by trade name, trademark, manufacturer, or otherwise does not necessarily constitute or imply its endorsement, recommendation, or favoring by the United States Government or any agency thereof. The views and opinions of authors expressed herein do not necessarily state or reflect those of the United States Government or any agency thereof.

DISCLAIMER

Portions of this document may be illegible in electronic image products. Images are produced from the best available original document.

DEVELOPMENT OF ENCAPSULATED LITHIUM HYDRIDE
SINK-SIDE THERMAL ENERGY STORAGE FOR
PULSED SPACE POWER SYSTEMS

D. G. Morris
J. P. Foote*
M. Olszewski
J. W. Whittaker†
Oak Ridge National Laboratory†
Oak Ridge, Tennessee 37831

Abstract

Value analysis indicates that inclusion of thermal energy storage (TES) as an element in a pulsed space power supply will reduce the mass of the heat rejection system. A candidate design for the TES component utilizes lithium hydride (LiH) encapsulated in 304L stainless steel or molybdenum in a packed-bed configuration with a lithium or sodium-potassium (NaK) heat transport fluid.

Critical concerns with this concept are the need to (1) accommodate shell stresses induced by volumetric expansion of the melting salt or surface gripping by the freezing salt and (2) minimize hydrogen loss through the shell due to LiH dissociation at high temperatures. Experimental observation of significant cracking of the LiH during cooling mitigates the first of these issues by providing a leakage path into the interior void as melting occurs at the salt-containment interface, thus

*Postgraduate student, University of Tennessee Space Institute, Tullahoma, TN 37388.

†Oak Ridge Y-12 Plant.

†Operated by Martin Marietta Energy Systems, Inc. under contract No. DE-AC05-84OR21400 with the U. S. Department of Energy.

By acceptance of this article the publisher of recipient acknowledges the U.S. Government's right to retain a nonexclusive, royalty-free license in and to any copyright covering the article.

allowing use of thin shells. Analysis indicates that, with 2% excess Li a 5-mil thick stainless steel shell or a 1-mil molybdenum shell is sufficient to achieve an acceptable hydrogen loss level.

1. Introduction

In space burst power applications, which require high power for relatively short durations, energy storage devices may be employed to reduce the size and mass of the thermal management system. This is accomplished by placing reject heat from the primary power system or other system components in the thermal storage system during the burst period. During the remaining non-power producing portion of the orbit, which can be an order of magnitude longer than the burst period, the stored heat is dissipated to space. The heat rejection rate is thus reduced and a smaller radiator is required. In concepts that are constrained by launch volume or deployed projection area, this can be a critically important attribute. Additionally, if the reduction in radiator mass is greater than the additional storage mass, overall system mass savings are possible.

LiH is the best candidate for use in power system sink-side thermal energy storage applications due to its superior heat storage properties and convenient melt temperature. The heat storage capacity of LiH is at least a factor of two greater than other materials one could consider for the application (e.g., lithium fluoride, magnesium chloride, aluminum, or magnesium). To maximize storage density, both sensible and latent modes of heat storage are used.

This paper focuses on the use of encapsulated LiH shapes in a packed-bed storage unit with Li or NaK as the heat transport fluid. Analytical and experimental development work associated with the concept is described. Since the program is in its early stages, the work has addressed basic feasibility issues associated with the use of encapsulated LiH shapes (principally spheres). These issues include shell stress induced by phase-change during heating, hydrogen diffusion through the encapsulating shell, heat transfer limitations due to poor conductivity of the salt, void behavior, and material constraints. The impact of these factors on the design of encapsulated LiH spheres has been evaluated analytically and experimentally.

2. System Concept Analysis

System value analysis was performed to determine, in a preliminary manner, the minimum storage density required for the encapsulated LiH packed-bed storage concept to be attractive (based on a total system mass criterion). A scoping design analysis was then conducted to determine the design conditions necessary for the storage unit to meet the required storage density. These design requirements were then used to set the goals for the development effort.

Value Analysis

A simplified schematic of a no effluent space power system employing an encapsulated LiH packed-bed for sink-side thermal storage is shown in Fig. 1. Depending upon the application, the source could be nuclear, solar or chemical. Power conversion could be accomplished using dynamic systems such as Brayton or Rankine cycles or static

systems such as thermionics. Engineering details necessary to integrate the storage system with the various power conversion options are beyond the scope of this study and have therefore not been delineated. However, it appears that thermionic conversion may be best suited to accommodate variable temperature storage.

Previous analysis¹ identified and examined the major parameters affecting the value of storage and demonstrated that the optimum storage minimum temperature was in the 500 to 700 K range. Thus, the value analysis performed to set research goals was limited to this range for the lower operating temperature of the store. The crossover time, plotted in Fig. 2 as a function of storage density, is defined as the time at which the storage and radiator-only systems are of equal mass. For pulse times less than the crossover time the storage system is lighter with the benefit of storage increasing as the pulse time decreases. To have reasonable applicability to space burst power needs it was decided that a crossover time of at least 500 s would be desirable. Thus, with an assumed radiator specific mass of 20 kg/m², the minimum system storage density was fixed at 3 MJ/kg.

Storage System Conceptual Design

Preliminary system conceptual designs were prepared for the proposed packed-bed storage system. System storage densities were calculated for several design options. Li and NaK were examined as the heat transport fluids. Also, the storage medium was examined using hydrides of naturally occurring Li (92.5% Li⁷, 7.5% Li⁶; denoted Li-7 in paper) and the isotope Li⁶. Preliminary information indicates that Li⁶ hydride possesses the same molar properties as Li-7 hydride. Thus, on a mass

basis the heat of fusion and specific heat will be 12% higher for Li⁶ hydride. It was assumed that the LiH spheres were encapsulated with a 0.013-cm (5-mil) thick stainless steel shell (this represents a design goal). As is shown later in the paper, a 5.1-cm diam sphere provides the optimal energy storage density for a 500-s pulse. With this design the shell accounted for about 18% of the sphere mass. Packing densities of 60 and 75% were examined.

As indicated by the results of the design analysis (see Table 1), Li is the preferred thermal transport fluid since all designs yield system storage densities in excess of 3 MJ/kg. Not surprisingly, the use of Li⁶ hydride is also preferred because of its enhanced storage density. Thus, it was concluded from the analysis that the design goal for the encapsulating shell wall thickness should be fixed at 0.013 cm for spheres with a diameter of 5.1 cm.

3. Development Issues and Evaluation

Thermal Assessment

A two-dimensional finite difference heat transfer computer code is being developed to model the thermal performance of LiH encapsulated in a spherical shell.² The numerical model will account for natural convection in the melt and the effect of the void which accompanies LiH phase-change (LiH volumetrically contracts 20% during solidification). The model uses the "enthalpy" method to account for phase-change in the salt. In the enthalpy method, the location of the phase-change front is not determined directly but is inferred from the energy content of the material. The computer program solves the fully implicit form of the

Table 1. Storage system operational energy densities (MJ/kg)

Minimum store temperature (K)	Encapsulated LiH system									
	LiH only		Li-7				Li ⁶			
	Li-7	Li ⁶	75%		60%		75%		60%	
			NaK	Li	NaK	Li	NaK	Li	NaK	Li
500	6.96	7.96	4.06	4.83	3.32	4.48	4.60	5.44	3.75	5.00
600	6.42	7.34	3.74	4.44	3.05	4.09	4.24	5.00	3.45	4.57
700	5.80	6.63	3.38	4.00	2.75	3.65	3.84	4.50	3.11	4.09

Note: "LiH only" gives maximum theoretical storage density of LiH alone without encapsulating shell or other structures for comparison purposes.

heat balance equations. The fully implicit formulation is used to avoid stability problems associated with the explicit solution and to minimize the difficulty in implementing a natural convection model. Heat balance equations are solved in radial-azimuthal coordinates with axial symmetry by line relaxation.³ Temperatures are scaled so the scaled temperature (T') at the melt point (T_{MP}) is zero:

$$T' = T - T_{MP} \quad , \quad \text{with } T_{MP} \approx 962 \text{ K}$$

Energy content is scaled so the energy content (E) of the solid at the melt point is zero. Therefore,

$$E = C_S T' \quad \text{For } T' < 0$$

$$E = C_L T' + H_{SL} \quad \text{For } T' > 0$$

where C_S and C_L are the specific heats of the solid and liquid, and H_{SL} is the heat of fusion (≈ 2.85 MJ/kg). When a given node has $0 < E < H_{SL}$, the temperature is fixed at zero until enough heat is added or removed so $E > H_{SL}$ or $E < 0$.

Results of calculations were checked against those from the explicit HEATING6 (Ref. 4) code, and agreement was found to be satisfactory. Earth-based experiments (and therefore under the influence of earth's gravity) have been planned to provide data for validation of the thermal model.

During the development of the two-dimensional thermal model, simplified one-dimensional finite difference models have been developed and used for micro-gravity (i.e., space) scoping assessments. These models have been primarily used to study the heatup portion of the thermal

cycle since it is the design limiting factor. Results from the models were compared to an analytical solution for a one-dimensional, constant density Stefan problem for a sphere,⁵ and were found to be in good agreement.

In the one-dimensional heatup analyses, several assumptions have been made that will require verification with the two-dimensional model and experimental data (ideally with micro-gravity data). The first assumption involves the location of the void in the solid material and its influence on convective heat transfer. The behavior of the void during solidification is not well understood. Preliminary analysis indicates that in the case of uniform cooling in micro-gravity, a spherical void will form in the center of the container;² this assumption is made in the present study. In this case, melt convection is expected to be small and is conservatively neglected; however, convection will be rigorously treated in the two-dimensional model. The second assumption concerns how the phase-change volumetric expansion is accommodated. Since the conceptual design envisions the use of rigid spherical containment shells, volumetric expansion must be handled internally. The volume expansion could be accommodated by crushing the solid LiH inward into the void. Whether or not this is a realistic possibility with a practical shell thickness depends on the compressive strength of the solid LiH, but in any event it provides a limiting case for the heat transfer study. Alternatively, the excess liquid could leak through the solid into the void. This would likely occur if there are cracks in the solid. The two scenarios comprise the "crush" and "leak" models, respectively. In the leak model, the means by which the

excess liquid makes its way through the solid is not considered. It is assumed that liquid at the fusion temperature appears in a freezing volume at the inner surface of the solid. In reality, the phase front at the inner surface of the solid may not be uniform since the liquid passes through localized cracks in the solid. The processes involved in the two models are illustrated in Fig. 3.

The crush and leak thermal models were used to determine the thermal response of single spheres of encapsulated LiH exposed to liquid metal convection. In the study, the liquid metal temperature was changed instantaneously from 700 to 1100 K which simulates heat rejection to the packed-bed (initially at 700 K) during the burst period. Based on theoretical relationships for liquid metal flowing past a single sphere,⁶ an average convection coefficient of $17 \text{ kW/m}^2\text{-K}$ was used for spheres in a packed-bed. The mass of LiH in the spheres was selected to completely fill the sphere volume when melted. The encapsulating shell was taken to be stainless steel, with a wall thickness of 0.013 cm (5 mils). Properties of the shell material and solid and liquid LiH were considered to be constant.

During the early stage of the melting process, the two models give very similar results, but as the process continues the rate of melting predicted by the leak model begins to exceed that of the crush model. This difference increases with time, due primarily to two effects. The conduction path through the liquid is shorter in the leak model. In addition, some heat is carried along with the liquid that leaks through the solid and thus bypasses the conduction path through the solid.

Figure 4 shows the results of calculations performed using the leak model. These results indicate that the optimal sphere size depends upon

the length of the burst period. With reference to Fig. 4, in moving to the right of the optimal sphere size, less of the available LiH storage capacity is utilized; in moving to the left of the optimal size, a larger shell parasitic mass penalty is incurred as the spheres decrease in size. The increase in optimal sphere size with burst period occurs simply because more time is available to transfer heat into the LiH.

Shell Stress

As mentioned previously, the void is expected to be located in the sphere center following cooldown in a micro-gravity environment. During subsequent heating, the liquid LiH expands against the shell and solid LiH. Figure 5 presents the calculated thermal response of a 5.1-cm diam sphere of encapsulated LiH when suddenly exposed to liquid metal convection. The initial temperature of the sphere was 700 K, and the temperature of the liquid metal was 1100 K. Temperature profiles are shown for the initial phase of the 500-s heatup. The curves were generated using the one-dimensional "crush" model. It can be seen that while the shell reaches the liquid metal temperature very rapidly, much of the solid is at a temperature significantly below the melt point when the LiH adjacent to the shell starts to melt.

An elastic stress analysis was performed to determine, in an approximate manner, the required shell thickness to prevent shell rupture. Molybdenum and 304L stainless steel (as described later, these are the leading candidate shell materials) were evaluated to determine the minimum required shell thickness. In this analysis it was assumed that the void forms in the sphere center, the LiH solidifies as a thick shell with no cracks, the containment shell is a thin shell, and thermal

stresses other than those resulting from phase-change are neglected. In addition, based on the thermal profiles in Fig. 5, the containment shell was assumed to be isothermal at the peak operating temperature, and the solid LiH was assumed to be isothermal at the minimum storage temperature.

As shown in Ref. 2, the minimum required shell thickness to prevent rupture is given by:

$$t = r/3 (\sigma_{\text{LiH}}/\sigma_{\text{S}})(\rho_{\text{L}}/\rho_{\text{S}}) ,$$

where

r = sphere radius

σ_{LiH} = LiH compressive strength

σ_{S} = shell tensile strength

$\rho_{\text{L}}, \rho_{\text{S}}$ = density of liquid and solid LiH.

Pressed LiH ultimate compressive strength data are given in Fig. 6 (left vertical axis) and as shown there is a strong temperature dependence.^{7,8} Table 2 presents LiH compressive strength at room temperature for pressed and sintered material.⁹ These data indicate that sintering results in large strength gains (about a factor of 1.7 greater for the 10 cycle sample). The sintered data are more likely representative of cast material, thus the data of Fig. 6 should probably be scaled upward by this factor. This has been done in the right vertical axis of Fig. 6.

At ~1100 K, the yield strength of 304L stainless steel¹⁰ and molybdenum¹¹ are taken as 69 (estimated) and 255 MPa (10 and 37 ksi), respectively. These properties do not reflect any effects of hydrogen or

Table 2. Compressive strength of LiH
at room temperature (Ref. 9)

Strength		Comments
MPa	psi	
100.7 ± 3.34	14,600 ± 485	Cold pressed
135.6 ± 34.61	19,670 ± 5,020	Cold pressed and sintered, 3 cycles*
110.0 ± 30.13	15,950 ± 4,370	Cold pressed and sintered, 5 cycles*
167.5 ± 6.31	24,300 ± 915	Cold pressed and sintered, 10 cycles*
	(95% confidence interval — room-temperature data)	*Blocks thermal cycled from room tem- perature to 866 K, specimens machined from sound, uncracked portion of blocks

Li on strength; however, for short lifetimes these effects are expected to be small.

Calculated achievable energy storage densities (i.e., includes shell, LiH, and Li; ~1.5 mole% "free" Li of total Li is needed to suppress hydrogen pressure resulting from LiH dissociation) based on the minimum required shell thickness determined as described above are presented in Table 3 for encapsulated LiH in spherical shells constructed of 304L stainless steel and molybdenum. Storage densities are based on a 500-s heatup period and use of naturally occurring Li and are shown for a range of minimum storage temperatures. The analysis assumed full utilization of the specific and latent heat capacities of the LiH. These results show that the required shell thickness is very large at low minimum storage temperatures, reflecting high LiH compressive strength. Obviously, with thick shells, only a very low energy storage density can be achieved. Even for minimum storage temperatures in the 500 to 700 K range, calculated shell thicknesses are much greater than permitted to obtain desired energy storage densities. As the LiH melt temperature is approached and the LiH strength is reduced, more reasonable shell thicknesses and energy storage densities can be achieved. For comparison purposes, energy storage with Li is shown in Table 3 where it is assumed that a shell with negligible mass can be used. Since no storage penalty is paid for an encapsulating shell, the storage density of Li decreases as the minimum storage temperature increases. The large change in storage density between 400 and 500 K occurs due to Li phase-change at 454 K. In the operating range of interest for the

Table 3. Energy storage densities of LiH
(stress constrained) and Li

Minimum store T (K)	Molybdenum shell			Stainless steel shell			Li (no shell) energy storage density (MJ/kg)
	Required shell thickness (cm)		Energy storage density (MJ/kg)	Required shell thickness (cm)		Energy storage density (MJ/kg)	
300	0.40	157	0.88	1.5	590	0.49	3.7
400	0.32	126	0.99	1.2	470	0.50	3.3
500	0.23	91	1.2	0.86	339	0.55	2.5
600	0.13	51	1.7	0.49	193	0.75	2.1
700	0.094	37	1.9	0.35	138	0.86	1.7
800	0.057	22	2.2	0.21	83	1.1	1.3
900	0.018	7.1	3.1	0.068	27	2.0	0.84
962	0.0009	0.35	3.7	0.0035	1.4	3.6	0.56

Note: Sphere diameter = 5.1 cm

LiH plus free Li mass = 37 grams

Pulse duration = 500 s

Li-7

minimum storage temperature (500 to 700 K), the achievable storage density is still well below that desired.

The storage densities presented in Table 3 can be compared to those shown in Table 1 for Li⁶ and Li-7 hydride, alone, to see the penalty paid for the encapsulating shell or using Li instead of LiH. Based on elastic stress analysis it appears that a desired shell thickness of ~0.0127 cm (5 mils) cannot be obtained in the temperature range of interest (even for a molybdenum shell, a material with substantial high temperature strength) if LiH forms a monolithic shell. However, it has been observed in tests conducted for this program² and others,^{12,13} that cracks form in the LiH during cooldown (as described later, preliminary indications are that LiH begins to crack on cooldown in the range of ~470 to 770 K, based on acoustic emission measurements). Thus, it is anticipated that cracks penetrating the solid LiH from the containment shell to the void will provide a path for expanding liquid LiH to reach the centrally located void during heatup. Hence, large hydrostatic forces are avoided, and a thin shell can successfully contain the LiH.

In the event that predictable, "well-behaved" cracks do not form, there are a series of potential design modifications to mitigate the stress problem. The following modifications have been investigated:²

1. providing internal fins made of the shell material,
2. using a non-wetting container material/coating or insulating part of the container surface, thus causing the void to form at the wall,
and
3. making the container flexible.

Although buckling of the shell due to the contraction of LiH during cooldown is a potential concern, no buckling analysis has been performed. Analysis would be of questionable value since buckling is sometimes observed experimentally at only 10% of the predicted critical stress level. As described subsequently, buckling concerns have been alleviated to some extent due to successful thermal cycle testing of thin-wall spheres.

Hydrogen Diffusion

LiH tends to dissociate into Li and hydrogen gas as it is heated. To prevent LiH dissociation an overpressure of hydrogen is required. Free hydrogen diffuses through the shell and results in a loss of energy storage density. As described in Ref. 14, hydrogen diffusion (loss) can be estimated using the following equation:

$$H_2 \text{ loss} = \frac{S t A P^{0.5}}{d},$$

where

S = hydrogen permeability of the metal,

t = time,

A = surface area of the encapsulating metal,

P = hydrogen pressure, and

d = shell wall thickness.

The hydrogen permeabilities of clean 304L stainless steel and molybdenum at 760 mm Hg and ~1100 K are ~0.45 and 0.07 CC(STP)-mm/h-atm^{0.5}-cm², respectively.¹⁴ Using these permeabilities, hydrogen loss from LiH encapsulated in 304L stainless steel and molybdenum has been calculated for a 25 cycle lifetime.¹⁵ The calculations were performed for a sphere with

a diameter of 5.1 cm containing ~37 grams of LiH plus free Li (initial LiH mole fraction of total Li = 98.5%). In addition, calculations assumed the use of naturally occurring isotopic LiH, a thermal storage temperature range of 700 to 1100 K, and a pulse duration and orbit time of 500 and 5880 s, respectively. Phenomenologically, it was assumed that hydrogen diffusion occurred, calculated as previously described, when liquid or hydrogen gas contacted the container wall, and that on cooldown LiH freezes first and uniformly on the shell surface preventing further hydrogen diffusion (i.e., the LiH freezes over the entire shell surface which ultimately results in a central void).

Figure 7 presents the calculated loss in energy storage density for molybdenum and clean stainless steel shells 0.00254, 0.0127, and 0.0381 cm (1, 5, and 15 mils) thick. An acceptable limit of 5% has been established, somewhat arbitrarily, for the application. These calculations indicate that hydrogen loss through a 0.0127-cm (5-mil) thick clean stainless shell results in only a 2% storage density loss; however, the loss is a relatively high 8% when the shell thickness is reduced to 0.00254 cm (1 mil). On the other hand, molybdenum shells as thin as 0.00254 cm (1 mil) can be used with less than 2% loss in storage density.

Material Considerations

Successful encapsulation of LiH requires that the shell material be compatible with LiH, Li, and hydrogen since all three materials will be present in the capsule. Compatibility is required over the temperature range ~700 to 1100 K, where most of the exposure is at ~700 K. Since the system is expected to experience no more than 25 cycles over its

lifetime, relatively short life is required at high temperatures (i.e., above the LiH melt temperature).

Based on a review of relevant materials data from a variety of sources, it was concluded in Ref. 2 that 304L stainless steel and molybdenum are the leading candidate shell materials. Material considerations included compatibility of the candidates with LiH, Li, and hydrogen, and their ductility, strength, density, material cost, and ease of fabrication. The refractory metals niobium, tantalum, titanium, and zirconium have been eliminated from consideration due to hydrogen embrittlement. It was determined that silicon carbide (SiC) is not compatible with Li at ~1100 K. 304L stainless steel and molybdenum possess reasonable ductility and moderate density. Molybdenum has greater strength and better material compatibility than 304L stainless steel, but is more expensive to fabricate.

4. Experiments

Scoping Experiments

Initial scoping experiments have been performed using 304L stainless steel cylindrical and spherical containers (cans) containing LiH. The purpose of these experiments was to perform preliminary scoping tests of containments and gain experience in the thermal cycling of encapsulated LiH. The tests provided insights into container and weld survivability following phase-change and the location and shape of the void formed during LiH solidification.

The cans were filled with preoutgassed LiH powder (chemical analysis of similar samples indicated 99.16 mole % LiH of total Li). A

"fill-tube" attached to the top of each can permitted pressure monitoring. The fill-tube was connected through flexible tubing to a pressure gage, vacuum pump, and argon purge line. The can was placed in a stainless steel beaker and packed with magnesium oxide (MgO). A thermocouple was located adjacent to the outside of the LiH container about halfway up the side. The beaker was placed inside a small resistance heated furnace (~720 W) and the top of the furnace was covered with insulation.

Using the setup described above, three cylindrical can tests were performed. Two tests used cans of 2.54-cm length, 3.81-cm diam, and 0.089-cm (35-mil) wall thickness, filled with about 14 grams of LiH. Based on density considerations, containers would be ~90% full at the maximum anticipated experimental temperature (~1050 K). In the first test (test C-1), the can was cycled once from room temperature to ~1000 K. In the second test (test C-2), the can was cycled a total of four times over a two day period with two cycles performed each day. The second cycle performed each day was initiated from about 25 K below the melt point rather than after return to room temperature. Heating from about 25 K below the melt point to about 50 K above the melt point occurred over 1 h; the cooling process was also 1 h in duration.

Posttest examination of the cycled test C-1 and C-2 canisters showed that a single, continuous void formed near the top of the can in both tests. As shown in Fig. 8, the void in the test C-1 can was not symmetrically formed, suggesting that the can was not level during testing and/or that there existed some nonuniform heating/cooling. Radiographs of the test C-2 can showed a similar void shape and location.

Comparison of measurements of container diameter before and after tests C-1 and C-2 showed no measurable change. However, comparison of before and after top-to-top measurements for test C-2 showed that the top-to-top distance had decreased about 0.05 cm (20 mils) (similar data was not collected for test C-1). Since the top and bottom of the can were flat, these surfaces could easily be deformed, possibly by "gripping" or shrinkage forces generated by the LiH during cooldown. Based on visual observation, the welds performed without failure.

Test C-3 was not successfully completed due to a weld failure resulting from LiH weld contamination during capsule sealing.

In test S-1, a spherical container with a 4.6 cm diam and 0.0254 cm (10-mil) wall thickness was used. The primary objectives of the test were to examine void behavior in a "hot-full" container (i.e., the sphere was filled with ~29 grams of LiH to produce a sphere almost completely full of liquid at the highest temperature anticipated), and to determine the resistance of the thin-wall sphere to buckling during cooldown. Test S-1 was conducted in a similar fashion to the cylindrical can tests, however two additional thermocouples were used in the test. One was located in the fill-tube, about 5 cm above the top of the sphere, while the other thermocouple was positioned inside the sphere to measure the LiH temperature. The sphere was heated through one thermal cycle. Shortly after apparently melting all of the LiH, the tube thermocouple temperature rose 53 K over a 5-min period, while the other temperature readings changed only slightly, indicating LiH had entered the ~0.64-cm inside diameter tube. Based on posttest radiographs, the resulting void shape is sketched in Fig. 9. It can be seen that frozen

LiH remained in the fill-tube. The mechanism for this apparent "crawling" behavior is not currently understood, but is being investigated. Posttest examination revealed no container deformation.

In test S-2, a spherical capsule identical to that used in test S-1 was sealed (the fill-tube was welded closed) and successfully cycled once from room temperature to 1100 K. Li was added to the LiH to prevent high hydrogen pressure associated with LiH dissociation or resulting from the decomposition of impurities [e.g. lithium hydroxide (LiOH) to lithium oxide (LiO₂); $\text{LiH} + \text{LiOH} \rightarrow \text{LiO}_2 + \text{H}_2$]. The Li/LiH mixture consisted of 5 mole % free Li and 95 mole % Li as LiH. Prior to sealing, the capsule loaded with the Li/LiH mixture was heated to ~770 K to outgas the system. The outgassing operation was performed using the same experimental apparatus as was used in the can tests. Peak gas evolution occurred in the temperature range 570 to 610 K and suggests the origin was the reaction of LiOH with LiH mentioned above, which is known to occur in this temperature range.¹³ At 770 K the minimum pressure achieved was 11 microns of Hg. Following cooldown to room temperature, the fill-tube was pressed flat and welded to form a seal. The capsule was then placed in a heavy vessel containing MgO along with thermocouples, and the assembly placed in a large resistance heated furnace (6 kW). Due to the large thermal inertia of the system, the heating and cooling rates were much slower than in previously described tests. The cooling rate just after LiH solidification at 962 K down to 600 K was ~75 K/h versus ~150 K/h in previous tests. Examination of the capsule following cycling revealed that the capsule experienced no significant deformation. As in test S-1, the void was located in the

top of the capsule with similar shape; however, it was a little larger at the the top and had a disconnected, less distinct secondary void beneath it.

The results of tests S-1 and S-2 indicate that thin-wall spheres can resist buckling due to LiH contraction on cooldown. In all tests conducted for the program, extensive cracking was observed (visually or radiographically) in the cast LiH after cooldown (for example, see Fig. 8), and is most easily seen in radiographs. Cracking appears to depend on cooling rate; significantly fewer cracks formed in test S-2 than in the other tests, presumably resulting from the slower cooldown rate.

Acoustic Emission Monitoring

In order for cracks in the LiH to provide the needed stress relief during heatup, cracking must initiate above the minimum storage temperature (500 to 700 K). Acoustic Emission (AE) monitoring of LiH during thermal cycling was performed to determine at what temperature (or within what temperature range) cracks form.

Tests were performed with 0.0254-cm (10-mil) and 0.0635-cm (25-mil) thick 304L stainless steel cylinders of 2.54-cm length and 3.81-cm diam. The cylinders were thermally cycled in a similar fashion to the previously described cylindrical can tests. An AE transducer (piezoelectric crystal) was attached via a spring clip to the can fill-tube just above the top cover of furnace insulation. Thus, the transducer was not exposed to high temperature; however, the transducer was in sufficient mechanical contact with the can to be sensitive to AE during thermal cycling. An empty can (10-mil wall thickness) was first cycled

three times to determine background noise. While AE was emitted during cycling with the empty can, the strength and frequency of this noise was significantly less than that observed in the thermal cycling with the LiH filled can. Tests examining LiH AE were conducted with a can (25-mil wall thickness) loaded with 13.5 grams of LiH to provide a hot liquid fill fraction of ~80%. Can wall thickness differences between the empty and LiH filled can are thought to result in insignificant AE differences. Four thermal cycles were performed with the LiH filled can. To assess the effect of cooldown rate on LiH cracking, the rate was varied from ~150 K/h in the first two cycles, to ~300 K/h in the third and fourth cycles over the temperature range 600 to 962 K. The latter rate is representative of application requirements.

Figure 10 represents selected test results from one of the two prototypical cycles. Temperature (measured at the surface of the can at its vertical centerline) and AE are shown as a function of time during cooldown. AE is presented in terms of root-mean-squared (RMS) voltage, which provides a measure of the energy content of individual events (AE producing occurrences). The results indicate the initiation of some relatively high energy AE shortly after 0.7 h at ~770 K. Although not shown, AE increased in frequency and magnitude as cooldown proceeded; in addition, high energy AE was observed in the heatup of LiH from room temperature to ~550 K. It was also observed that more high energy AE was produced at the higher cooldown rate, thus suggesting that more cracking accompanies faster cooldowns. This observation is consistent with the results of scoping experiments discussed previously where LiH

cracking in test S-2 (~75 K/h cooldown) was noted to be less than in the other tests (~150 K/h cooldown).

Following a study of all the data, it was hypothesized that the high energy AE represents LiH cracking.¹⁶ Based on this assertion, it was concluded that LiH crack initiation during cooldown occurred in the temperature range 470 to 770 K, where the higher initiation temperature occurred at the higher (prototypic) cooldown rate.^{16,17} Thus, some cracking of the LiH can be expected in the energy storage application.

5. Conclusions

Based on preliminary value analysis, it was concluded that system storage densities of 3 MJ/kg or greater are required to produce significant mass savings in the heat rejection system. Achievement of this goal using the encapsulated LiH packed-bed concept depends critically on the feasibility of thin shell (<5 mils) encapsulation. The most promising system uses Li⁶ hydride as the storage medium with a packing density of 75% and Li as the thermal transport medium.

The feasibility of thin shell encapsulation has been investigated through experimental and analytical studies. A group of feasibility issues have been identified and discussed:

1. phase-change induced shell stress on heatup,
2. hydrogen diffusion and loss,
3. LiH heat transfer, and
4. material considerations.

The key issue of concern is the possible large shell stress induced during heatup. Elastic stress analysis indicated that very thick shells

would be required to prevent shell rupture, if the LiH formed a structurally sound shell during solidification. However, cracks in the LiH have been experimentally observed during cooldown which will likely mitigate shell stresses and permit the use of a thin shell.

Based on projected system requirements, a 0.0127 cm (5 mil) thick 304L stainless steel shell will provide sufficient hydrogen containment to prevent significant hydrogen loss, and associated loss of storage density. Due to molybdenum's lower hydrogen permeability, a molybdenum shell as thin as 1 mil could be used without significant hydrogen loss.

Heat transfer considerations indicate that the optimal sphere size increases in diameter from 5 to 8.5 cm as the pulse duration increases from 500 to 1500 s.

Based on material consideration, 304L stainless steel and molybdenum are leading candidate shell materials. Material consideration included compatibility of the candidates with LiH, Li, and hydrogen, and their ductility, strength, density, material cost, and ease of fabrication.

Initial scoping experiments have been completed for cylindrical and spherical shells containing LiH. Four thermal cycles were successfully completed in a low heat flux furnace with cylindrical cans with 0.0889-cm (35-mil) and 0.0635-cm (25-mil) wall thicknesses and one thermal cycle was successfully completed with two, 0.0254-cm (10-mil) thick spherical containers. Results of the thin-wall sphere tests provide some confidence that a 0.0127-cm (5-mil) thick spherical shell can be used without suffering buckling failure. Post-test examination of all

canisters tested showed the presence of numerous cracks in the LiH.

Based on the results of AE tests, LiH crack initiation occurs at ~770 K at application cooldown rates; thus, some cracking of the LiH can be expected in the application.

Acknowledgments

This work was sponsored by the Air Force Wright Aeronautical Laboratories, AeroPropulsion Laboratory. The work was performed under Interagency Agreement DOE 40-1508-84. Extensive Y-12 Plant experience with LiH was utilized to accomplish experimental objectives; W. L. Asbury, C. E. Irwin, and G. E. Wrenn have been particularly helpful.

References

1. Olszewski, M. and Morris, D. G., "Value of Energy Storage in Pulsed Space Power Systems," ORNL/TM-10530, January 1988.
2. Morris, D. G., Foote, J. P., and Olszewski, M., "Development of Encapsulated Lithium Hydride Thermal Energy Storage for Space Power Systems," ORNL/TM-10413, December 1987.
3. Patankar, S. V., "Numerical Heat Transfer and Fluid Flow," Hemisphere Publishing Co., 1980.
4. Elrod, D. C. et al., "HEATING6; A Multidimensional Heat Conduction Analysis with the Finite Difference Formulation," NUREG/CR-0200, October 1981.
5. Stewartson, K. and Waechter, "On Stefan's Problem for Spheres," Proc. of the Royal Society of London A.348, 415-526 (1976).
6. Hsu, C. J., "Heat Transfer to Liquid Metals Flowing Past Spheres and Elliptical Rod Bundles," Int. J. Heat Mass Transfer," Vol. 8, 303-315 (1965).
7. Anon., "Nuclear Propulsion Program Engineering Progress Report," PWAC-604, October 1-December 31, 1960, Pratt and Whitney Aircraft Corp., January 31, 1961, pp. 88-89.
8. Anon., "Nuclear Propulsion Program Engineering Progress Report," PWAC-611, January 1-March 31, 1961, Pratt and Whitney Aircraft Corp., April 18, 1961.
9. Welch, Frank H., "Properties of Lithium Hydride III. Summary of GE-ANP Data," XDC-61-5-67, Aircraft Nuclear Prop. Dept., General Electric Co., May 1961, p. 7.

10. Hoke, John H., "Mechanical Properties of Stainless Steels at Elevated Temperatures," pp. 21-1-21-20 in *Handbook of Stainless Steels*, Peckner, Donald, and Bernstein, I. M., editors, McGraw-Hill Book Company, 1977.
11. Anon., "Refractory Metals and Custom Fabrication," Rembar Company, Inc.
12. Waldrop, F. B., "Lithium Hydride as a Mobile Neutron Shield," Y-1191, Union Carbide Nuclear Corp., February 24, 1958, p. 7-8.
13. Smith, Roger L. and Miser, James W., "Compilation of the Properties of Lithium Hydride," NASA-TM-X-483, 1962.
14. Flint, P. S., "The Diffusion of Hydrogen Through Materials of Construction," KAPL-659, Knolls Atomic Power Laboratory, December 14, 1951.
15. Mahefkey, E. T., Air Force Wright Aeronautical Laboratories, Aero-Propulsion Laboratory, Dayton, Ohio, personal communication to D. G. Morris, Oak Ridge National Laboratory, Martin Marietta Energy Systems, Inc., Oak Ridge, TN, January 1987.
16. Whittaker, J. W., "Characterization of Acoustic Emission from Thermally-Cycled Lithium Hydride," Y-DW-767, October 1987.
17. Whittaker, J. W. and Morris, D. G., "Characterization of Acoustic Emission From Thermally Cycled Lithium Hydride," presented to the 31st meeting of the Acoustic Emission Working Group, UCLA, March 22-24, 1988.

FIGURE CAPTIONS

Fig. 1. Simplified schematic of power system employing encapsulated LiH sink-side thermal storage.

Fig. 2. Heat rejection system crossover time for selected minimum storage temperatures.

Fig. 3. Schematics of crush and leak thermal models.

Fig. 4. Thermal energy storage in spherically encapsulated LiH.

Fig. 5. Temperature profiles in spherically encapsulated LiH during the initial phase of the charge cycle.

Fig. 6. Pressed and estimated-cast LiH ultimate compressive strength (Refs. 7, 8).

Fig. 7. Energy storage density loss resulting from hydrogen diffusion.

Fig. 8. Opened test C-1 cylindrical can following thermal cycle.

Fig. 9. Sketch of LiH freeze pattern observed in spherical container test S-1.

Fig. 10. Acoustic emission from encapsulated LiH during cooldown.

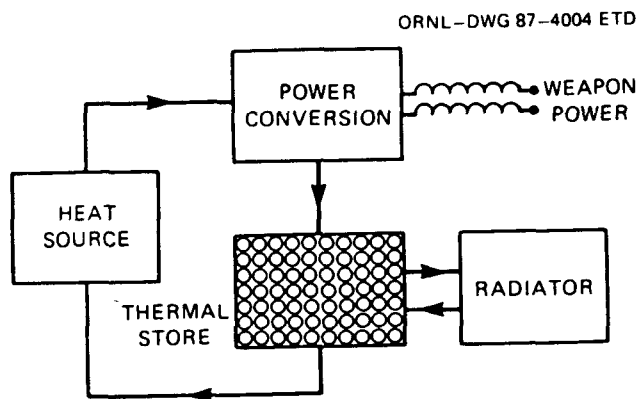


Fig. 1. Simplified schematic of power system employing encapsulated LiH sink-side thermal storage.

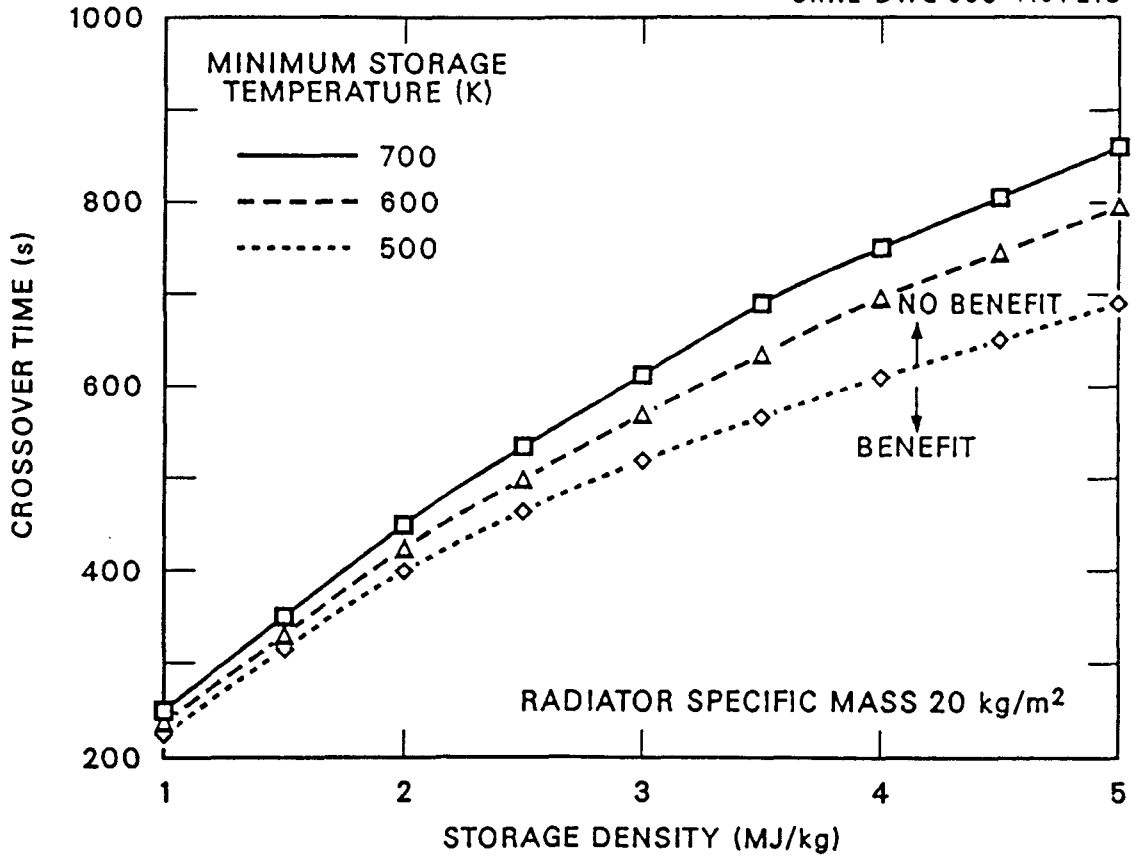


Fig. 2. Heat rejection system crossover time for selected minimum storage temperatures.

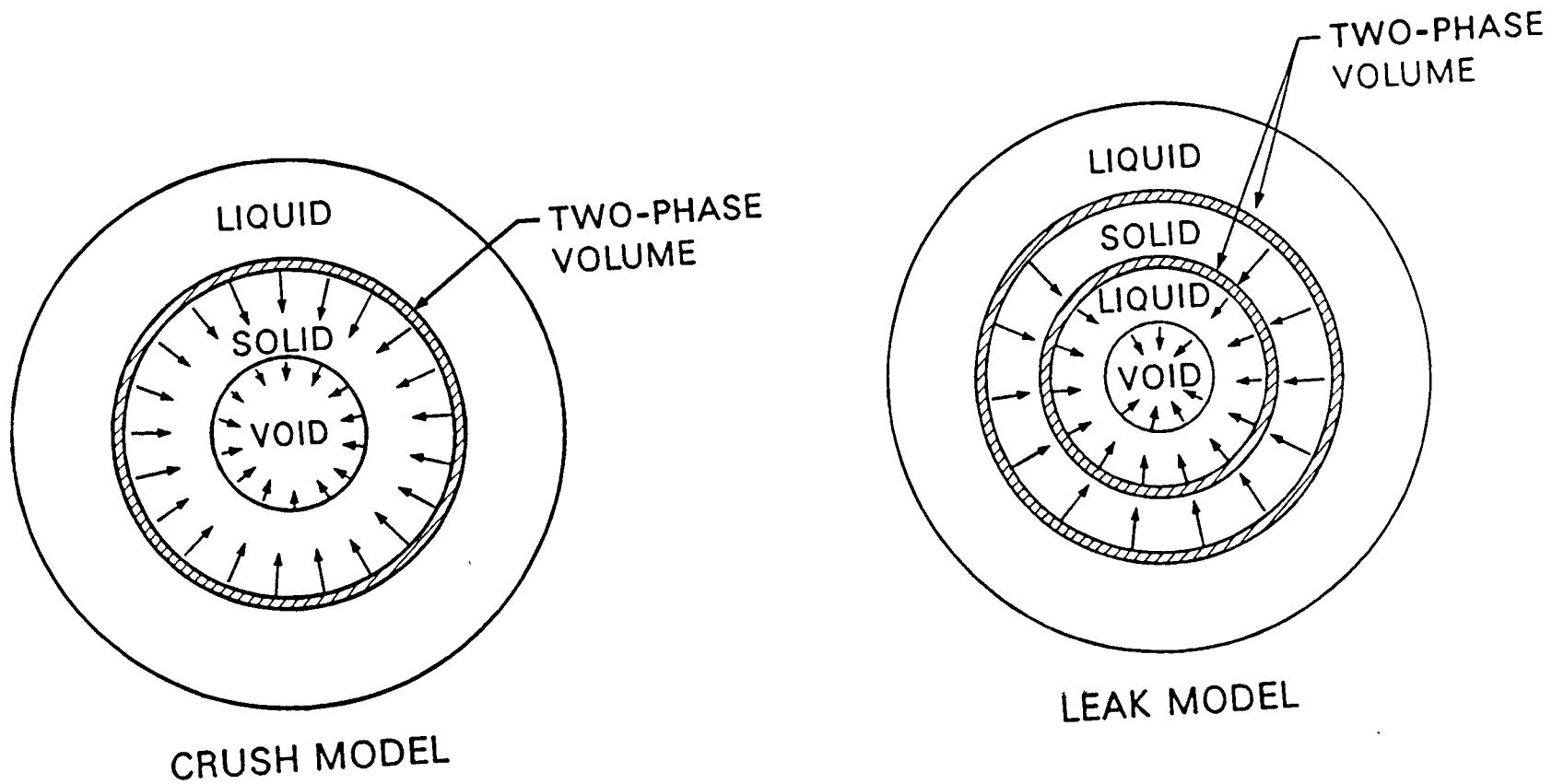


Fig. 3. Schematics of crush and leak thermal models.

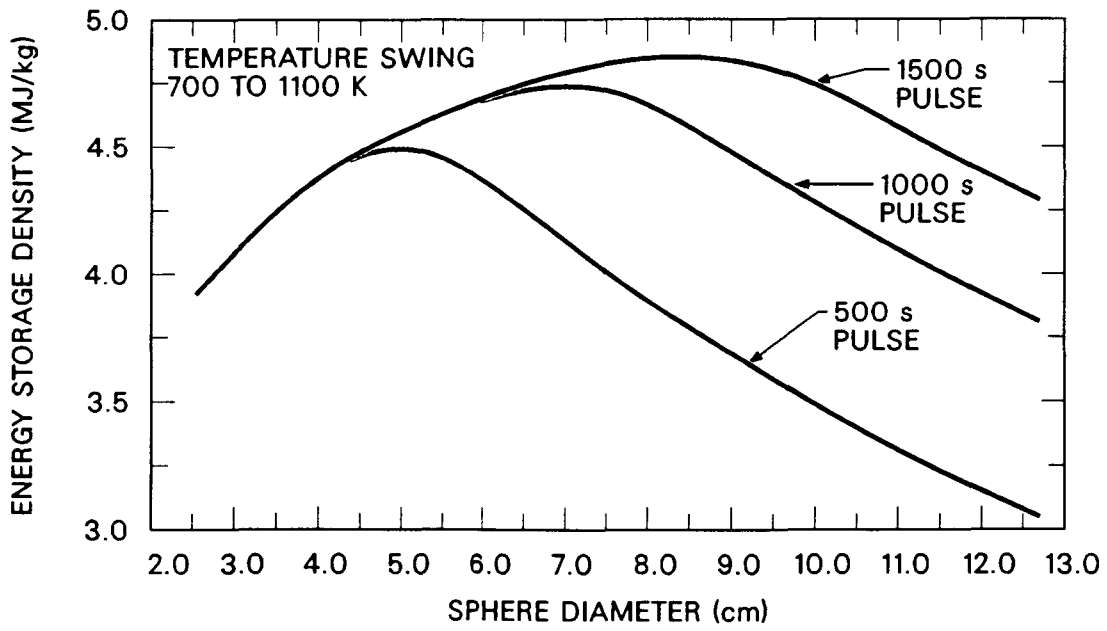


Fig. 4. Thermal energy storage in spherically encapsulated LiH.

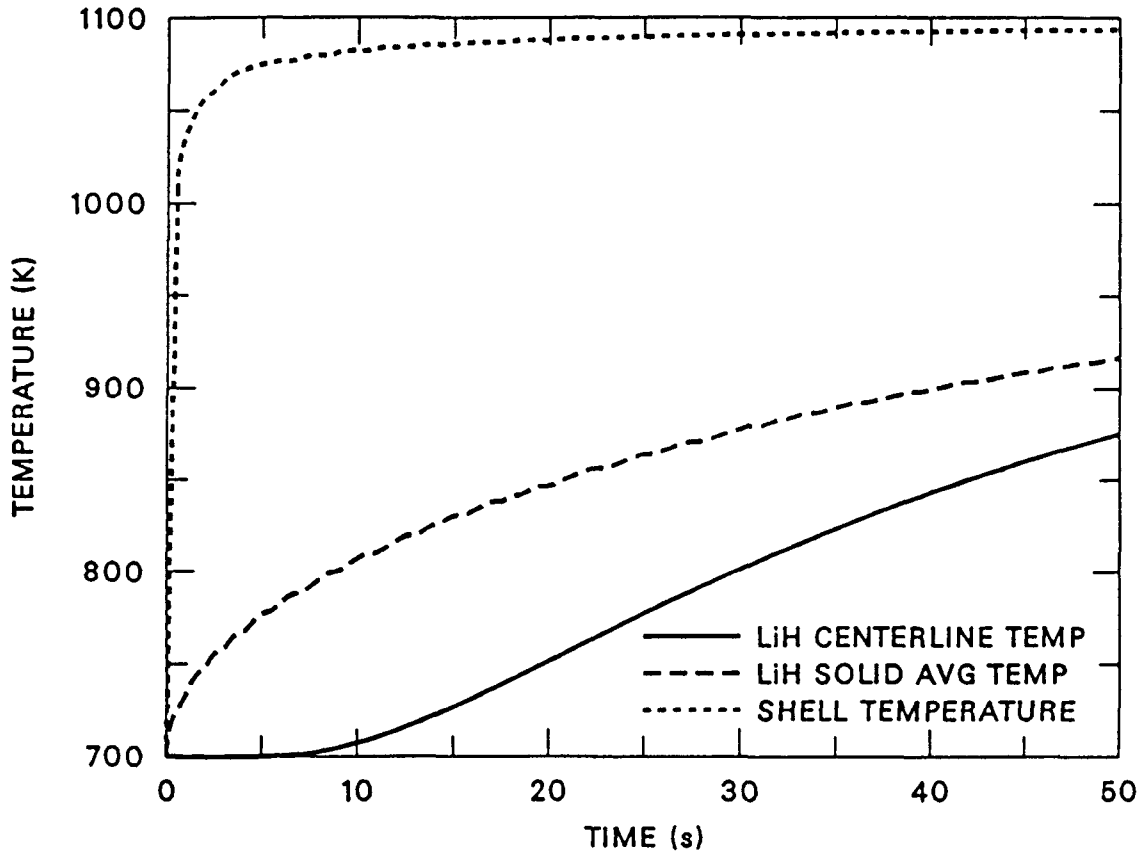


Fig. 5. Temperature profiles in spherically encapsulated LiH during the initial phase of the charge cycle.

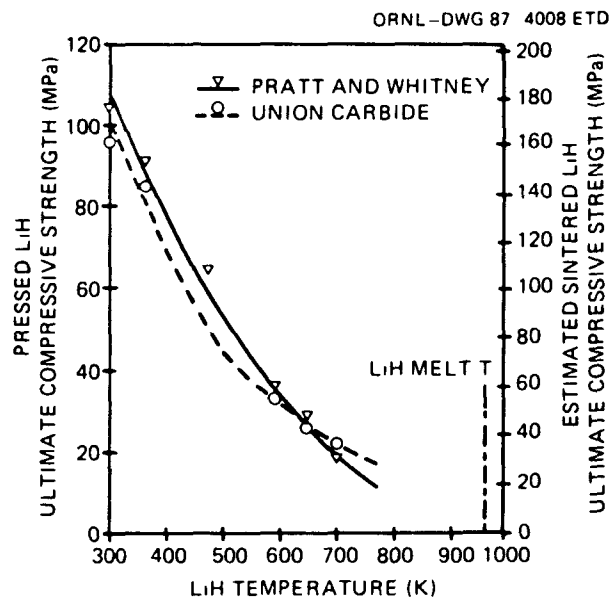


Fig. 6. Pressed and estimated-cast LiH ultimate compressive strength (Refs. 7, 8).

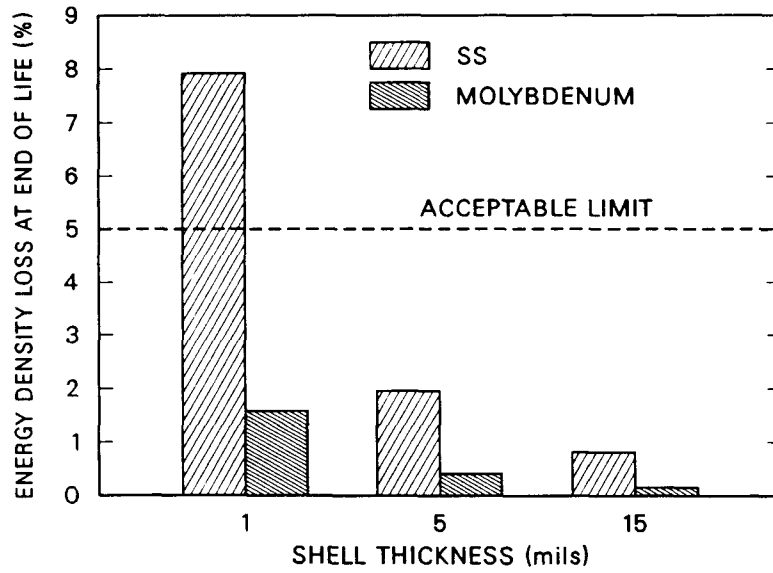


Fig. 7. Energy storage density loss resulting from hydrogen diffusion.

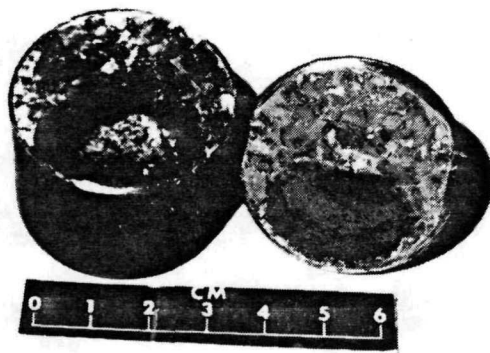


Fig. 8. Opened test C-1 cylindrical can following thermal cycle.

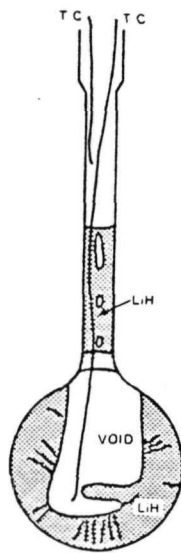


Fig. 9. Sketch of LiH freeze pattern observed in spherical container test S-1.

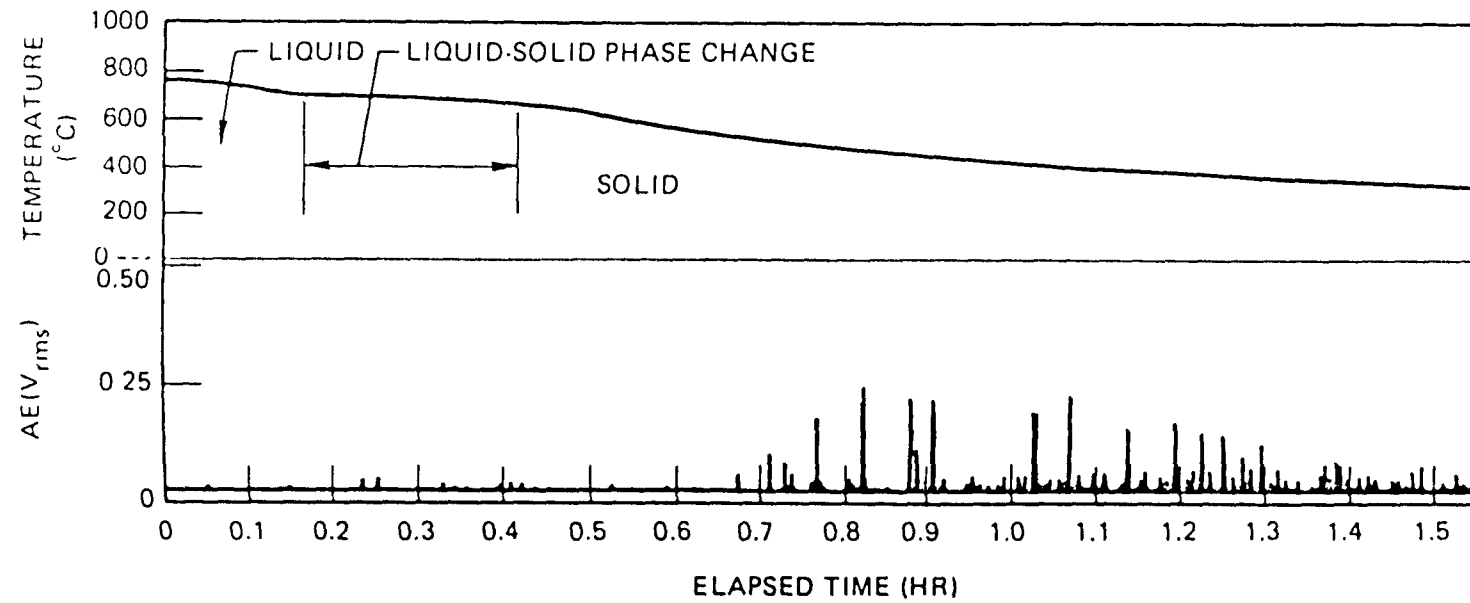


Fig. 10. Acoustic emission from encapsulated LiH during cooldown.